

Mechanism of Hyaluronan Degradation by *Streptococcus pneumoniae* Hyaluronate Lyase

STRUCTURES OF COMPLEXES WITH THE SUBSTRATE*

Received for publication, December 17, 2001, and in revised form, April 30, 2002
Published, JBC Papers in Press, May 3, 2002, DOI 10.1074/jbc.M112009200

Mark J. Jedrzejewski^{‡§¶}, Luciane V. Mello^{||}, Bert L. de Groot^{**}, and Songlin Li[§]

From the [‡]Children's Hospital Oakland Research Institute, Oakland, California 94609, the [§]Department of Microbiology, University of Alabama at Birmingham, Birmingham, Alabama 35294, ^{||}National Centre of Genetic Resources and Biotechnology, Cenargen/Embrapa, 70770-900 Brasília, Brazil, and ^{**}Max Planck Institute for Biophysical Chemistry, 37077 Göttingen, Germany

Hyaluronate lyase enzymes degrade hyaluronan, the main polysaccharide component of the host connective tissues, predominantly into unsaturated disaccharide units, thereby destroying the normal connective tissue structure and exposing the tissue cells to various endo- and exogenous factors, including bacterial toxins. The crystal structures of *Streptococcus pneumoniae* hyaluronate lyase with tetra- and hexasaccharide hyaluronan substrates bound in the active site were determined at 1.52- and 2.0-Å resolution, respectively. Hexasaccharide is the longest substrate segment that binds entirely within the active site of these enzymes. The enzyme residues responsible for substrate binding, positioning, catalysis, and product release were thereby identified and their specific roles characterized. The involvement of three residues in catalysis, Asn³⁴⁹, His³⁹⁹, and Tyr⁴⁰⁸, is confirmed, and the details of proton acceptance and donation within the catalytic machinery are described. The mechanism of processivity of the enzyme is analyzed. The flexibility (allosteric) behavior of the enzyme may be understood in terms of the results of flexibility analysis of this protein, which identified two modes of motion that are also proposed to be involved in the hyaluronan degradation process. The first motion describes an opening and closing of the catalytic cleft located between the α - and β -domains. The second motion demonstrates the mobility of a binding cleft, which may facilitate the binding of the negatively charged hyaluronan to the enzyme.

Streptococcus pneumoniae colonizes predominantly the upper respiratory tract of humans and is a major human pathogenic bacterium. It is one of the key causes of life-threatening disease such as pneumonia, bacteremia, and meningitis (1). It also causes less threatening diseases that are, however, very prevalent like otitis media and sinusitis (2). Pneumococci interact with the host and its tissues through the surface sugars

* This work was supported by National Institutes of Health Grant AI 44079 (to M. J. J.). The costs of publication of this article were defrayed in part by the payment of page charges. This article must therefore be hereby marked "advertisement" in accordance with 18 U.S.C. Section 1734 solely to indicate this fact.

The atomic coordinates and structure factors (code 1Loh and 1Lxk) have been deposited in the Protein Data Bank, Research Collaboratory for Structural Bioinformatics, Rutgers University, New Brunswick, NJ (<http://www.rcsb.org/>).

¶ To whom correspondence should be addressed: Children's Hospital Oakland Research Institute, 5700 Martin Luther King Jr. Way, Oakland, CA 94609. Tel.: 510-450-7932; Fax: 510-450-7910; E-mail: mjedrzejewski@chori.org.

(capsule) and a variety of usually surface-exposed protein molecules. These interactions are essential for the full pathogenicity of these bacteria and are likely involved in the disease-causing processes. The proteins known to be involved in this interaction include, among others, hyaluronate lyase (3, 4), pneumolysin (5), pneumococcal surface protein A (6), and pneumococcal antigen A (7, 8).

S. pneumoniae hyaluronate lyase (SpnHL)¹ primarily degrades hyaluronan (HA), the predominant polysaccharide component of animal and human connective tissues and the nervous system, into unsaturated disaccharide units as the end products (9). Cells in the connective tissues are embedded in the strikingly viscoelastic HA matrix. Hyaluronan is a polymeric glycan composed of linear repeats of a few hundred to as many as 20,000 or more disaccharide units of glucuronic acid and *N*-acetylglucosamine. The glycosidic linkage present within the disaccharide unit is β -1,3, whereas the disaccharide units are connected with the β -1,4-glycosidic linkage. The HA metabolism seems to be more significant than the metabolism of other polysaccharides *in vivo* due to the large turnover of this sugar. In human, one-third of the HA (about 5 g) is turned over daily (10). The rapid turnover rate facilitates the use of HA and its degradation products in many physiological processes, such as cell differentiation and development (11), cell proliferation, recognition, locomotion, and the immunological responses (12).

Enzymes of either mammalian (including host or human enzymes) or bacterial origin degrade HA at the β -1,4-linkage exerting the endo- and exogenous pressures on the host. Bacteria secrete hyaluronate lyases to degrade HA, and these enzymes usually produce unsaturated di-, tetra- (HA₄), or hexasaccharides (HA₆). The mechanism of this degradation by *Streptococcus* species hyaluronate lyase, which produces primarily unsaturated disaccharides of HA, 2-acetamido-2-deoxy-3-*O*-(β -D-glucopyranosyluronic acid)-D-glucose, as the end products, was recently proposed and involves the elimination reaction introducing an unsaturated bond to the product (9). Mammals, on the other hand, express hyaluronidases to degrade HA and to produce relatively longer oligosaccharides (13). The detailed atomic mechanism of HA degradation by mammal hyaluronidases is still largely unknown due, in part, to the lack of structural information. This process likely relies on the displacement mechanism based on hydrolysis, similar to

¹ The abbreviations used are: SpnHL, *S. pneumoniae* hyaluronate lyase; ED, essential dynamics; MD, molecular dynamics; HA, hyaluronan; HA₄, tetrasaccharide of HA; HA₆, hexasaccharide of HA; HA1, and HA2, HA3, positions of hyaluronan building blocks of disaccharide for HA numbered from the reducing toward the non-reducing end; PAD, proton acceptance and donation.

that of cellulases, to degrade the HA substrate (13). Mammalian hyaluronidases (mainly bovine hyaluronidase) are, however, widely used in clinics, for example as an additive to the local anesthesia for the fast spreading and penetration of medications through tissues (14, 15).

The structure of the native SpnHL (9) and its complex with the disaccharide products of HA degradation (16) were recently reported. This structural information together with further characterization of the enzyme (17, 18) allowed for the formulation of the proposed mechanism of HA degradation (9, 13). Briefly, the mechanism of catalysis, termed proton acceptance and donation, involves a five-step process involving neutralization of the carboxylate of a glucuronic moiety, extraction of a proton from C-5 followed by a double bond formation in the glucuronate and breaking of the β -1,4-glycosidic linkage. Additional comparison to other enzymes degrading glycans like *Streptococcus agalactiae* hyaluronate lyase (19), *Flavobacterium heparinum* chondroitin AC lyase (20), and *Sphingomonas* species alginate lyase A1-III (21) allowed for generalization of the pneumococcal enzyme mechanism and suggested a similar mechanism of action for these additional enzymes (13). Here we report the structures of the *S. pneumoniae* hyaluronate lyase complexes with its substrates, the tetra- and hexasaccharide units of hyaluronan, and we discuss their implications for the mechanism of action of the enzyme.

EXPERIMENTAL PROCEDURES

Enzyme and Substrate Preparation, Crystallization of Complexes, and Collection of Diffraction Data—The SpnHL Y408F mutant cloning, overexpression in *Escherichia coli* (pMJJ004), and purification were reported previously (9, 22). The mutant enzyme was concentrated to 5 mg/ml in 10 mM Tris-HCl, pH 7.4, 2 mM EDTA, and 1 mM DL-dithiothreitol and stored at -80°C until their use. The tetra- and hexasaccharide substrates were also obtained as described previously (17, 18). To prevent degradation they were stored frozen at -80°C in 10 mM Tris-HCl buffer, pH 8.0, until their use.

The crystals of Y408F mutant version of SpnHL were obtained using the same conditions as for the native enzyme crystals (100 mM sodium cacodylate buffer, pH 6.0, 2.9 M ammonium sulfate) but with the addition of 5 mM EDTA (23). Crystallization of Y408F mutant enzyme was accomplished using the vapor diffusion hanging drop method in 24-well Linbro culture plates using equal volumes of the protein sample and the reservoir solution (2 μl of each) at 22°C (24, 25). The protein and reservoir solution were mixed and equilibrated against 1.0 ml of reservoir solution. Diffraction quality rectangular block shaped crystals of Y408F (0.5 \times 0.3 \times 0.3 mm) were grown within several days. The crystals of Y408F SpnHL were then soaked at room temperature with 20 mM tetra- and hexasaccharide substrates (both in 10 mM Tris-HCl buffer at pH 8.0) for 10 h directly before the x-ray diffraction data collection. The crystal soaking solution contained the crystallization conditions (100 mM sodium cacodylate buffer, pH 6.0) with increased concentration of the precipitation agent, ammonium sulfate, to 3.2 M.

The crystal was cryo-protected using the same conditions as for the native crystals (23) and flash freezing them at -170°C in a nitrogen flow using a Cryostream Cooler (Cryosystems, Oxford, UK). The diffraction data sets were collected using synchrotron radiation at the wavelength of 1.0 \AA at the 19-BM beamline at the Argonne National Laboratory, Advanced Photon Source, Structural Biology Center using an Oxford 3 \times 3 charged-coupled device detector. The diffraction limits of the crystals were 1.52- and 2.0- \AA resolution for the tetra- and hexasaccharide complexes, respectively. The data were processed and scaled using the HKL2000 package (26). The crystals of complexes were isomorphous to the native ones. The final data processing parameters are reported in Table I.

Determination of Structures of Complexes with Tetra- and Hexasaccharides—The native SpnHL crystal structure without water molecules (9) was used as the model for the complex structure solution. The R_{free} flag was assigned to 1 (1,249 reflections) and 2% (1,205 reflections) reflections for the tetra- and hexasaccharide complexes, respectively, to validate the refinement progress (27). Initially, a round of rigid body refinements using only the model was performed using X-PLOR (28). The Tyr⁴⁰⁸ was manually mutated to Phe using the O program (29). Refinements progress using program X-PLOR with the positional and simulated annealing protocols (28, 30) and was traced using inspection

on graphics with program O (29). The structures were refined against 124,927 and 60,437 reflections for the tetra- and hexasaccharide complexes, respectively, and utilizing all data from 50 \AA to the highest resolution available and a $2\sigma(F)$ cut-off (Table I). The electron density for the substrates was then clearly identified, and the incorporation of the substrates into this density was followed. The topologies and parameter files for both substrates were manually created following our earlier studies with disaccharide substrates and carefully corrected to reflect ideal stereochemical values (16). Additional refinements including individual restrained B-factor refinements, inspection, and manipulation of structure on graphics using O together with incorporation of water molecules placed into 3σ peaks in σ -A weighted $F_o - F_c$ maps following standard criteria were performed. After refinement, water molecules whose positions were not supported by electron density, at 1σ contouring, in σ -A weighted $2F_o - F_c$ maps were deleted. A variety of stereochemical (31) and other analyses (29, 32) was periodically performed in order to locate possible model errors. The tetra- and hexasaccharide substrate molecules and 685 and 590 waters were incorporated, respectively, into the final structures of these two complexes. Final refinement parameters are reported in Table I.

Flexibility Analysis and CONCOORD Simulations—The CONCOORD program (33, 34) generates uncorrelated protein structures fulfilling a set of upper and lower interatomic distance limits. These limits are derived from experimental structures through measurement of interatomic distances and prediction of the interaction strength of the involved atoms. Thus, the separation of strongly interacting atoms was allowed to vary only slightly from the observed value, whereas weaker interactions have more relaxed limits. Special consideration was given to interacting atoms within the same secondary structure element in order to ensure the preservation of secondary structure. Although detailed aspects of dynamic variation may not be reproduced by this method, good qualitative agreement has been found between the results of the conventional molecular dynamics and CONCOORD simulations (33–35). Trajectories containing 500 conformations were calculated.

Essential Dynamics Calculations—The essential dynamics (ED) was performed by Gromacs 3.0 (36, 37). This method is based on the diagonalization of the covariance matrix of atomic fluctuations, which yields a set of eigenvalues and eigenvectors (38). The eigenvectors indicate directions in a $3N$ dimensional space (where N = number of atoms) and describe concerted fluctuations of the atoms, constructed such that the amount of fluctuation along a small number of eigenvectors is maximized. The eigenvalues reflect the magnitude of the fluctuation along with the respective eigenvectors. The central hypothesis of this method is that the motions along the eigenvectors with the largest eigenvalues are essential for describing the function. The motion along any desired eigenvector can be inspected by projecting the frames from the trajectory onto that eigenvector.

The figures were prepared using Ribbons (39), Grasp (40), O (29), and Molscrip (41).

RESULTS AND DISCUSSION

Choice of the Mutant Enzyme and Substrates—The native *S. pneumoniae* hyaluronate lyase enzyme used in our studies was active in the crystallized form. When crystal was combined with the hyaluronan substrates, the degradation to disaccharides was observed. This led to three-dimensional structures for the complexes identical to that of the complex with the disaccharide product reported earlier (16) (data not shown). The presence in crystals of EDTA, to chelate divalent cations such as calcium, which are required for full enzyme activity, was not sufficient to totally prevent substrate degradation by the enzyme (data not shown). The use of an inactive mutant of the enzyme was, therefore, necessary to obtain complexes of the hyaluronan-derived substrates larger than disaccharide HA with the enzyme. Our earlier studies (9) showed that the Y408F mutant of the enzyme is essentially inactive, and for this reason this mutant form of the enzyme was chosen for our studies. Indeed, the tetra- and hexasaccharide HA substrates were not degraded by the enzyme during complex formation in the crystals. The Y408F mutant enzyme consisted of residues Ala¹⁶⁸ to Gln⁸⁹² of the full-length protein and a C-terminal His₆ tag engineered for the ease of purification (22).

The tetra- and hexasaccharide hyaluronan substrates were chosen because our earlier modeling studies (9, 16) suggested

TABLE I
Crystallographic statistics of diffraction data and structure refinement of *S. pneumoniae* hyaluronate lyase complexes with tetra- and hexasaccharide hyaluronan substrates

	SpnHL-HA ₄ complex	SpnHL-HA ₆ complex
Space group	P2 ₁ 2 ₁ 2 ₁	P2 ₁ 2 ₁ 2 ₁
Unit cell dimensions (Å)	<i>a</i> = 83.7, <i>b</i> = 103.8, <i>c</i> = 101.3	<i>a</i> = 83.7, <i>b</i> = 103.6, <i>c</i> = 101.3
Resolution range (Å)	50.00–1.52	50.00–2.00
Measured reflections	904,361	407,437
Unique reflections	124,927	60,259
Completeness (last shell) (%) ^a	93.1 (49.8)	99.9 (99.4)
R _{merge} ^b (last shell) (%)	8.0 (61.1)	16.7 (91.0)
Final model	719 amino acids, 585 waters	721 amino acids, 590 waters
R _{cryst} ^c (last shell)	19.00 (33.0)	22.4 (32.4)
R _{free} ^d (last shell)	23.9 (39.5)	24.3 (38.4)
R.m.s.d. ^e bonds (Å)	0.006	0.007
R.m.s.d. ^e angles	1.235	1.305
Average B-factors (Å ²)		
Whole protein	45.08	26.24
α-Domain	48.40	29.18
β-Domain	41.36	23.20
Water molecules	53.48	34.22
Substrates	67.27	20.21

^a The last shell is defined as 1.52–1.59 Å for the tetrasaccharide complex and 2.0–2.07 Å for the hexasaccharide complex.

^b $R_{\text{merge}} = \sum |I_i - \bar{I}| / \sum I_i \times 100$ where I_i is the intensity of an individual reflection, and \bar{I} is the mean of all reflection.

^c $R_{\text{cryst}} = \sum |F_p| - |F_{\text{calc}}| / \sum |F_p| \times 100$ where F_p and F_{calc} are the measured and the calculated structure factors, respectively.

^d R_{free} is as defined by Brunger and Krukowski (55).

^e R.m.s.d., root mean square deviation.

that they should fit entirely within the catalytic cleft of the enzyme and not interfere with the crystallization process. These truncated hyaluronan substrates were produced in milligram quantities from a human umbilical cord hyaluronan by a controlled degradation with *Streptomyces hyalurolyticus* hyaluronate lyase as reported previously (9, 42, 43). This enzyme is an eliminase and produces tetra- and hexasaccharides with an unsaturated uronic acid at their non-reducing end as the final degradation products. These products were identified using ion spray mass spectrometry experiments.

Solution and Refinement of Structures of Complexes—The crystals of the inactive Y408F mutant form of the enzyme were obtained using the hanging drop vapor diffusion method and essentially the original crystallization condition of the native enzyme reported previously (23). The crystals of the complexes were obtained by soaking the Y408F mutant enzyme crystals with 20 mM tetra- and hexasaccharides of HA for a relatively short time directly before the freezing the crystals and/or diffraction data collection. The best soaking time was determined to be 10 h. The diffraction data were collected and processed, and structures were solved and refined as described under “Experimental Procedures.” The data in Table I show well refined structures with excellent stereochemistry. In a Ramachandran plot (31), a majority of the residues for the tetra- and hexasaccharide complexes are located in the most favored areas and none in the disallowed or generously allowed areas. These crystal structures were solved at 1.52- and 2.0-Å resolution, respectively (Fig. 1). The tetrasaccharide complex structure contains residues Lys¹⁷¹ to Lys⁸⁸⁹, and three N-terminal residues and three C-terminal residues together with the C-terminal His₆ tag were not seen in the electron density. For the hexasaccharide complex one additional residue on each end of the molecule was partially located in the electron density maps and was modeled as alanine. The electron density was very clear for the entire structure of both complexes, including the substrate molecules, with the exception of the very N and C termini of the enzyme where disorder was evident (Fig. 2). The structure of the complex with the tetrasaccharide contained 685 ordered water molecules, whereas that of hexasaccharide includes 590 water molecules in addition to protein and substrate molecules. For both substrates, there was only one substrate molecule bound per molecule of the enzyme.

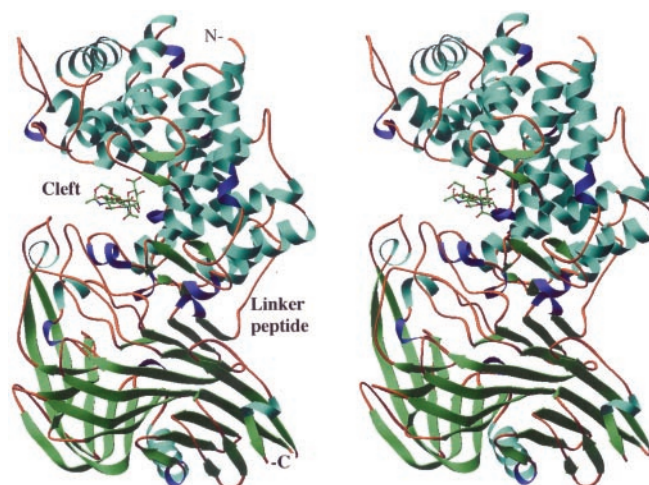


FIG. 1. Ribbon drawing of *S. pneumoniae* hyaluronate lyase complex with the tetrasaccharide hyaluronan substrate. Both domains of the enzyme are shown, the α-helical domain (α-domain, top) and the β-sheet domain (β-domain, bottom), as well as the cleft with the bound tetrasaccharide of hyaluronan. The structure of the enzyme is color-coded by the secondary structure elements. The N and C termini are labeled as N- and -C.

Description of the Complex Structures—The protein components of both crystal structures of the complexes are nearly identical to one another as well as to the structure of the native enzyme (9). Briefly, the protein molecules are built from two structural domains connected only by one short and flexible linker peptide consisting from 11 amino acid residues (Fig. 1). The structural domains are the N-terminal α-helical domain (α-domain) and the C-terminal β-sheet domain (β-domain). The α-domain is composed of 13 helices arranged in a α5/α5-barrel structure (Fig. 1). The larger end of this barrel is shaped as a deep and elongated cleft, which faces the β-domain. The β-domain is primarily composed of five anti-parallel β-sheet structures forming a β-sandwich. A part of this domain is in close proximity to the cleft present in the α-domain. However, its contribution to the shape of the cleft is minimal and restricted to two loops between the β-sheets of the β-domain, which contribute to the shape of a part of one edge of the cleft (Fig. 1). The cleft contains the substrate-binding site and catalytic res-

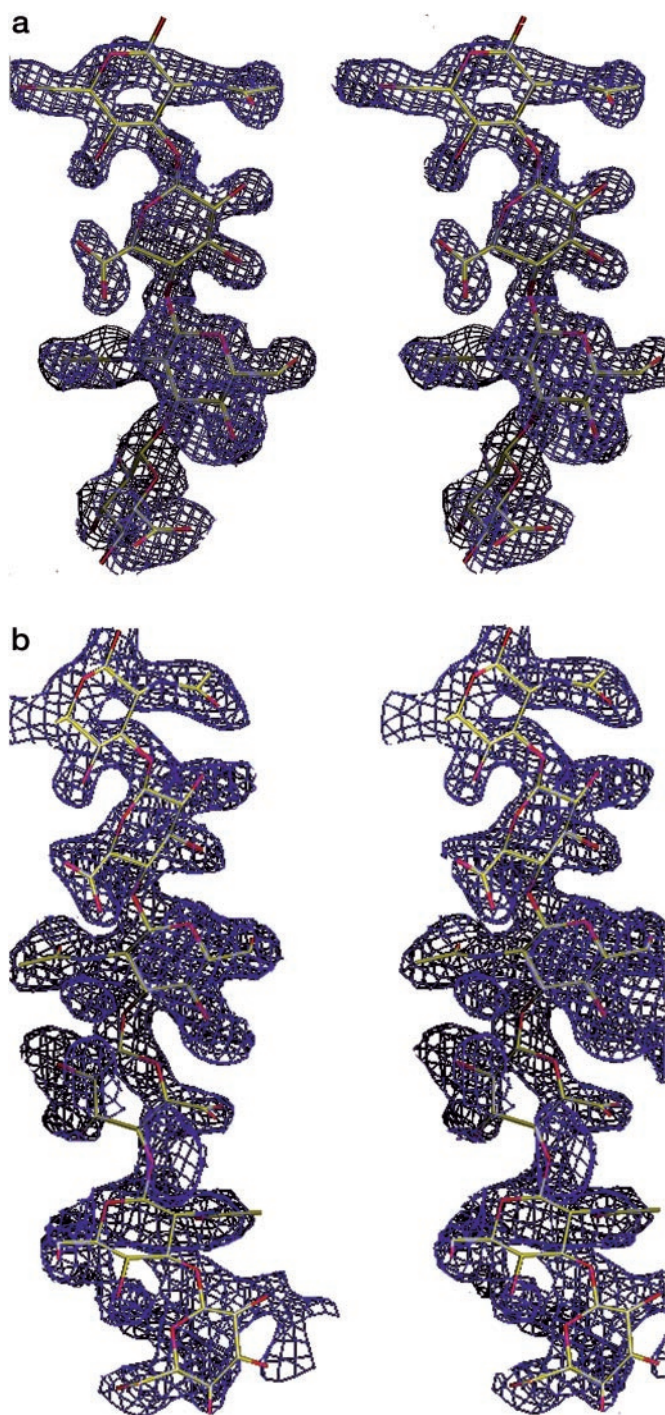


FIG. 2. **Electron density maps for the substrate molecules in the structure of their complexes with the enzyme.** The figure shows a stereo view of the $2F_o - F_c$ electron density maps contoured at 1σ level. *a*, electron density for tetrasaccharide hyaluronan. *b*, electron density for hexasaccharide hyaluronan.

idues. The detailed description of the native structure has been reported elsewhere (9).

Structure and Conformation of the Tetra- and Hexasaccharide Hyaluronan Substrates—The structures of both tetra- and hexasaccharide HA substrates are similar in their orientation and placement in the cleft of the enzyme (Figs. 2 and 3). The tetrasaccharide position in the cleft essentially overlaps with a portion of the hexasaccharide substrate at its reducing end. In naming the disaccharide units of HA from the reducing to the non-reducing end, this portion consists of HA1 and HA2. HA3

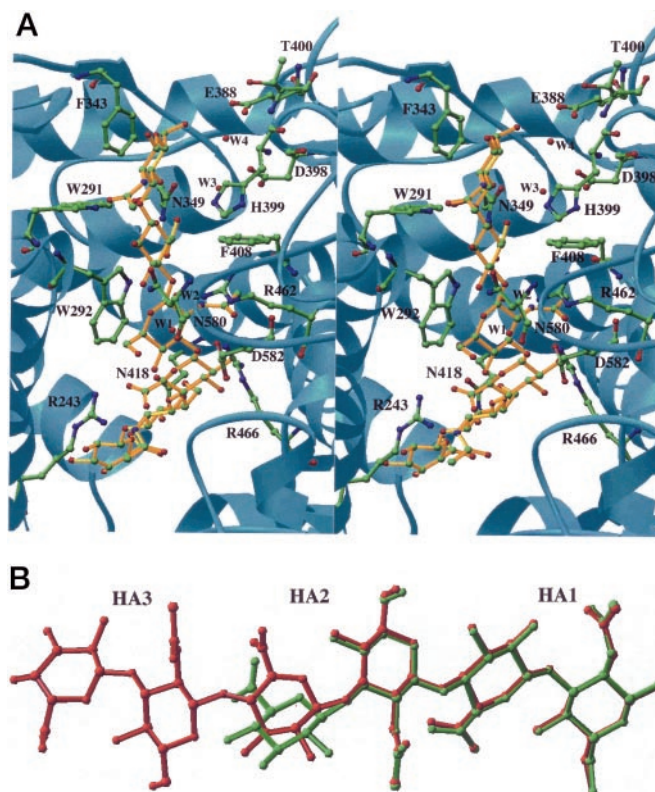


FIG. 3. **Protein-substrate interface in the structures of complexes.** The hexasaccharide hyaluronan substrate molecule is colored in light brown and the protein ribbon in blue. The substrate and selected residues are shown in a ball and stick style using standard colors for spheres representing atoms. *a*, a stereo view of enzyme-hexasaccharide hyaluronan interface. *b*, overlap between the tetra- and hexasaccharide substrates bound in the cleft of the enzyme. Hexasaccharide hyaluronan is colored in red and tetrasaccharide in green.

is unique to the hexasaccharide complex. The sugar rings (*N*-acetyl- β -D-glucosamine and β -D-glucuronate rings) of both substrates are in chair conformations with the exception of the terminal sugar rings of the unsaturated β -D-glucuronates located at the nonreducing end of both substrates (which are unsaturated due to the presence of the double bond between C-4 and C-5 introduced during substrate production, HA3 for hexasaccharide and HA2 for tetrasaccharide) that are in distorted half-chair conformations. Both substrates, including the sugar ring substituents, fit well within clearly defined electron density. The majority of substituents of the sugar rings was clearly identified in such densities. The current structures closely resemble and agree with our earlier modeling studies (9, 16) of both tetra- and hexasaccharides in the cleft of the native enzyme. There are number of interactions between the substrates and the enzyme residues including the catalytic, hydrophobic, positive, or negative patch residues. There are no predominant interactions responsible for substrate binding, rather the binding of the substrate is accomplished by numerous interactions of HA with multiple residues of the enzyme. Such binding is consistent with the processive character of the enzyme as described below.

The Catalytic Cleft and the Active Site—The substrate-binding cleft is located at the larger end of the $\alpha 5/\alpha 5$ barrel, and its surface is built primarily from loop areas between the helices of the α -domain. The only residues from the β -domain contributing to the cleft are two loops between β -strands, encompassing residues 578–583 and 766–771. The cleft dimensions are 30 Å in length, 10 Å in width, and 14 Å in depth. Such an elongated and relatively wide cleft allows for easy access of the elongated

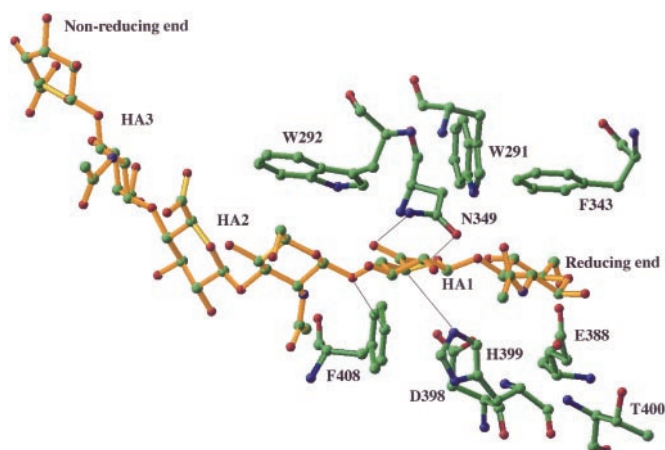


FIG. 4. Active center of *S. pneumoniae* hyaluronate lyase. The hexasaccharide substrate chain is shown with selected residues of the cleft: catalytic group (Asn³⁴⁹, His³⁹⁹, and Phe⁴⁰⁸ (Tyr⁴⁰⁸ was mutated to Phe for the current structural studies)), hydrophobic patch (Trp²⁹¹, Trp²⁹², and Phe³⁴³), and negative patch (Glu³⁸⁸, Asp³⁹⁸, and Thr⁴⁰⁰). Interactions of the catalytic group residues and their targeted substrate atoms are shown by lines. The substrate chain is shown in yellow, and enzyme residues are shown in standard colors corresponding to atom type. The reducing and non-reducing ends of the substrate are labeled. Both ends of substrates may extend to include longer polymeric hyaluronan chain. The β -1,4-glycosidic linkage between HA1 and HA2 positions is to be cleaved.

HA substrate. The surface of the cleft is highly electropositive due to the abundance of basic residues at its surface. Hyaluronan is electronegative due to the negative charges of the carboxylate groups along its chain, and it also has significant hydrophobic character (44). The charge complementarity between the cleft and HA allows for electrostatic interactions between the enzyme and the substrate resulting in substrate binding. The predominant features of the cleft are as follows: (a) multiple basic residues lining the cleft surface making it highly positively charged and thereby facilitating substrate binding; (b) a cluster of three negatively charged residues, Glu³⁸⁸, Asp³⁹⁸, and Thr⁴⁰⁰, located at the terminal part of the cleft that form a negative patch implicated in product release (reducing end of the bound substrate, see below); (c) three closely placed aromatic/hydrophobic residues, Trp²⁹¹, Trp²⁹², and Phe³⁴³, located next to the catalytic residues of the cleft and forming a hydrophobic patch that is implicated in precise positioning of the substrate for the catalysis; and (d) three residues, Asn³⁴⁹, His³⁹⁹, and Tyr⁴⁰⁸, that are proposed to be directly involved in catalysis (Figs. 3 and 4).

Based on our earlier site-directed mutation studies, a group of 5 residues was considered to affect directly the catalytic process with 3 of them involved in the catalytic process, Asn³⁴⁹, His³⁹⁹, and Tyr⁴⁰⁸, and the remaining 2, Arg²⁴³ and Asn⁵⁸⁰, involved in substrate binding. These five mutant enzymes were produced (R243V, N349A, H399A, Y408F, and N580A) and characterized kinetically, and the correlations between the kinetic properties and the structure were made (Fig. 3) (9, 17). Both the structure and the kinetic analysis of the three catalytic residues Asn³⁴⁹, His³⁹⁹, and Tyr⁴⁰⁸ were shown to be involved directly in catalysis, and their mutations caused significant changes in the K_m , V_{max} , and V_{max}/K_m kinetic parameters. Similarly, two additional residues, Arg²⁴³ and Asn⁵⁸⁰, were implicated in substrate binding and translocation but not catalysis (9, 17). The native enzyme obeyed Michaelis-Menten kinetics.

The degradation of HA is thought to be processive with the random initial endolytic enzyme binding to hyaluronan followed by exolytic degradation of the same substrate chain

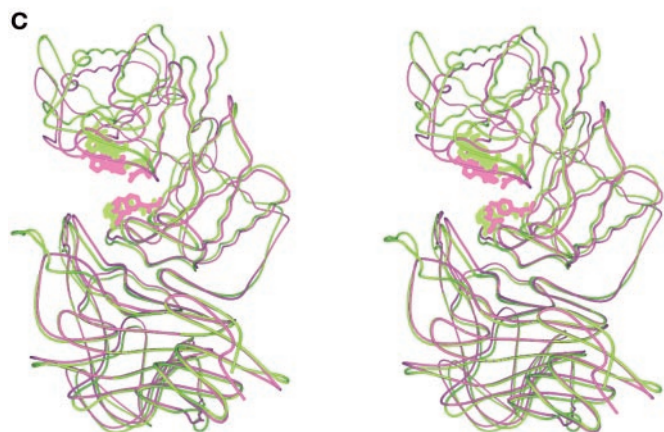
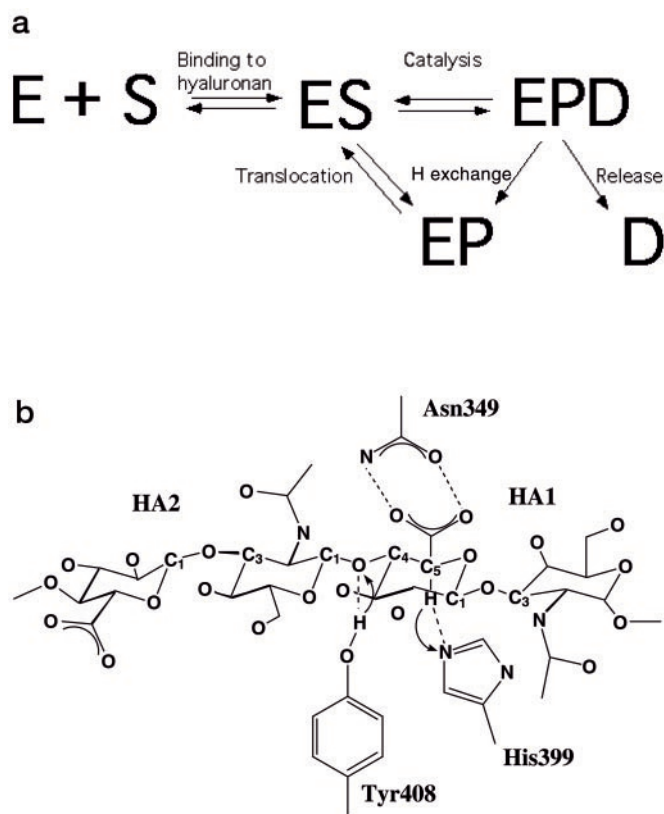


FIG. 5. Schematic diagrams of hyaluronan degradation. a, overall mechanism of hyaluronate lyase action. The abbreviations used are: E, enzyme; S, hyaluronan substrate; EPD, enzyme with bound truncated hyaluronan substrate and a disaccharide product; EP, enzyme with bound truncated hyaluronan substrate and disaccharide product released from the active site of the enzyme. b, the catalytic mechanism of hyaluronan degradation. The catalytic residues and their relative position to the substrate were shown to illustrate the mechanism of HA degradation as described in the text. The side chain position of Tyr⁴⁰⁸ has been modeled on the basis of the Y408F mutant structure. c, structural alignment of *S. pneumoniae* and *S. agalactiae* hyaluronate lyase. The pneumococcal enzyme is drawn in violet, and the *S. agalactiae* enzyme is shown in chartreuse. The catalytic residues of both enzymes are highlighted using the same colors. The similarity in the overall three-dimensional structures, sequence, and structure identity of the catalytic center suggest the same mechanism of action of both enzymes.

toward its non-reducing end until the whole substrate was degraded (Fig. 5) (17, 45). For the pneumococcal hyaluronate lyase, and for several other known bacterial hyaluronate lyases, the final degradation product is an unsaturated disaccharide derivative of hyaluronic acid (22). The analysis of the native structure, its modeled or x-ray crystal complex struc-

TABLE II
Selected interactions of hyaluronate lyase residues with the substrate molecules

The symbols assigned to the substrate atoms follow standard chemical nomenclature for sugar molecules.

Substrate/water atoms	Enzyme/water residues and atoms	Distance for HA ₄	Distance for HA ₆
NAc1 ^a of HA1			(Å)
C-3	Trp ²⁹¹ NE1	3.86	3.95
C-6	Phe ³⁴³ CD1	3.80	3.70
O-3	Trp ²⁹¹ NE1	2.87	2.89
O-4	Phe ³⁴³ CZ	3.94	4.00
O-5	Asn ³³⁶ NH2	3.56	3.66
O-6	Glu ³⁸⁸ OE2	3.83	3.94
O-7	Trp ²⁹¹ NE1	3.59	3.61
UA1 of HA1			
O-4 (glycosidic oxygen between HA1 and HA2)	Phe ⁴⁰⁸ CZ (Tyr ⁴⁰⁸ OH) ^b	4.63 (3.10)	4.55 (3.18)
	Arg ⁴⁶² NH2	3.02	3.16
	Wat ¹	4.04	4.07
	Wat ²	4.61	3.41
O-5	His ³⁹⁹ NE2	3.66	3.73
O-6 (glucuronate CO ₂)	Asp ³⁴⁹ OD1	3.12	2.98
O-7 (glucuronate CO ₂)	Asp ³⁴⁹ ND2	3.56	3.34
Wat ³	His ³⁹⁹ NE2	6.99	6.30
Wat ⁴	His ³⁹⁹ NE2	6.39	6.73
NAc2 of HA2			
O-3	Arg ⁴⁶⁶ NH1	3.34	3.22
	Arg ⁴⁶⁶ NH2	3.67	3.82
O-5	Trp ²⁹² CD2	3.83	3.89
O-7	Arg ⁴⁶⁶ NH2	2.94	2.97
UA2 of HA2			
O-2	Arg ⁴⁶⁶ NH1	2.63	3.74
O-6 (glucuronate CO ₂)	Arg ²⁴³ NH1	3.63	2.24
O-7 (glucuronate CO ₂)	Arg ²⁴³ NH2	3.63	2.90
NAc3 of HA3			
O-3	Arg ³⁰⁰ NH2	NA ^c	3.51
O-6	Asn ⁴¹⁸ OE1	NA	3.59
	Asp ⁴¹⁴ OD1	NA	3.52
UA3 of HA3			
O-2	Glu ²⁴⁶ OE2	NA	2.31
O-4	Lys ²⁵⁰ NZ	NA	2.93
O-6 (glucuronate CO ₂)	Asn ⁴¹⁸ NE2	NA	3.39
O-7 (glucuronate CO ₂)	Asn ⁴¹⁸ NE2	NA	3.34

^a UA1, UA2, and UA3 denote the β -D-glucuronic acid of HA1, HA2, and HA3, respectively, whereas NAc1, NAc2, and NAc3 denote *N*-acetyl- β -D-glucosamine of HA1, HA2, and HA3, respectively.

^b The distance in parentheses corresponds to the distance between the modeled Tyr⁴⁰⁸ OH atom position based on the native enzyme structure position of Tyr⁴⁰⁸ residue and the glycosidic oxygen of the corresponding complex structure.

^c NA, not applicable.

tures with substrates and products of degradation, mutation studies, and the kinetic analysis allowed for the formulation of a five-step catalytic process responsible for HA degradation. This process was proposed to consist from the following: (i) a hyaluronan substrate binding step, (ii) a catalytic step, (iii) hydrogen exchange with the water microenvironment, (iv) an irreversible product release step, and (v) a translocation of the remaining polymeric substrate step (Fig. 5a) (9). These steps are described in more detail below.

Hyaluronan Binding in the Substrate Binding Cleft of the Enzyme—In order for the hyaluronan degradation process to be feasible, the enzyme needs to bind to the substrate utilizing its elongated cleft. However, the immobilized structure of the enzyme in the crystals might not totally reflect the possible changes in and the dynamics of the structural properties of this enzyme. As shown below using a flexibility analysis based on dynamics calculations, the β -domain of the enzyme might have a significant degree of mobility with respect to the α -domain. Therefore, it is possible that the β -domain modulates the access of substrate to the catalytic cleft by opening up or closing down the entrance to this cleft (see below). The Asn⁵⁸⁰ residue of the β -domain contributes to the cleft formation in its narrowest part, and mutation of this residue to one with a smaller side chain, Gly, likely widens the cleft entrance. An N580G mutant showed significantly higher activity as the wild type enzyme (9, 17) suggesting that cleft opening had allowed for easier binding of the substrate. The K_m and V_{max} kinetic parameters of the

N580G mutant enzyme are 0.99 ± 0.22 mM and 725 ± 61 mmol/(min·mg), respectively. Corresponding values for the native enzyme were determined to be 0.08 ± 0.04 mM and 563 ± 18 mmol/(min·mg) (17). The comparison of these kinetic parameters clearly shows that the N580G binds the substrate with a lesser affinity ($V_{max}/K_m = 732$ for the mutant and 7038 for the wild type enzyme) but is a more efficient enzyme in translocating the nascent product/substrate (higher V_{max}), a property that may be directly related to the width of the cleft opening.

After the initial binding or docking of the substrate in the cleft, hyaluronan is precisely positioned along the cleft interacting predominantly with charged residues lining the cleft surface (9). The importance of this process is reflected by the loss of activity of the R243V mutant. As the current complex structures show, the Arg²⁴³ residue interacts directly with the carboxylate of the glucuronic acid moiety of the penultimate disaccharide (Table II and Fig. 3a) and as such has the ability to align the substrate directly along the cleft. Mutation of Arg²⁴³ to Val disturbs this precise alignment along the cleft axis, and the enzyme loses significant activity (17).

The substrate chain also is oriented such that the reducing end of the chain is located at the narrower end of the cleft where catalysis is performed (9, 16, 19). Such unidirectional binding of hyaluronan determines its direction of degradation by the enzyme from the reducing to the non-reducing end (see below). The positions of the three-disaccharide units of the HA₆ substrate bound in the cleft are termed HA1, HA2, and HA3

from the reducing to the non-reducing end of the substrate and similarly HA1 and HA2 disaccharide units for the HA₄ substrate.

Finally, directly next to the catalytic residues determined by our earlier research (9), there are three hydrophobic residues, Trp²⁹², Trp²⁹¹, and Phe³⁴³, creating a hydrophobic area in the cleft termed aromatic/hydrophobic patch (Fig. 4). These residues interact with the substrate utilizing the hydrophobic in-character sugar rings of the first and the penultimate disaccharide units of the substrates. Trp²⁹² interacts with the HA2 unit, whereas Trp²⁹¹ and Phe³⁴³ interact with the HA1 disaccharide unit of both the hexa- and tetrasaccharides. In this way, these three residues precisely position the substrate and its chemical groups in positions most suitable for catalysis performed by three catalytic residues Asn³⁴⁹, His³⁹⁹, and Tyr⁴⁰⁸ (Figs. 4 and 5*b*). The binding of the substrate in the opposite direction is not favored because it creates significant steric clashes between the enzyme and the substrate, and the catalytic residues are not positioned favorably with respect to the substrate for catalysis.

Catalytic Cleavage of the Glycosidic Bond—We have proposed previously (9), based on the structure of the native enzyme and its modeled complex structure with the tetra- and hexasaccharide units of HA, its complex structure with the disaccharide product of degradation (16) and mutation studies (9, 17) that the catalytic residues are Asn³⁴⁹, His³⁹⁹, and Tyr⁴⁰⁸ (Fig 5*b*). The current complex structures with the tetra- and hexasaccharide HA units confirm our earlier conclusions. As shown in Table II, Asn³⁴⁹ directly interacts in a bidentate fashion with the carboxylate group of the glucuronate moiety of HA1. This interaction allows Asn³⁴⁹ to act as a partial electron sink by attracting the electronegative charge of the carboxyl group of HA1 away from the C-5 of glucuronate. This process leads to acidification of the C-5 hydrogen that normally has a high p*K*_a value, which is estimated to be in the range from 29 to 32 (46). As a consequence, His³⁹⁹ acting as a base can withdraw this hydrogen, and the C-5 is rehybridized to the *sp*² hybridization. In the complex structures His³⁹⁹ is in direct contact with the C-5 of the glucuronate moiety (Table II), which supports our suggestion. At the same time Tyr⁴⁰⁸ acts as an acid and donates hydrogen to the glycosidic oxygen leading to cleavage of its β-1,4 covalent glycosidic bond between HA1 and HA2. The C-4 is then rehybridized to the *sp*² hybridization, and a double bond is formed between C-4 and C-5 (Fig. 5*b*).

To avoid substrate degradation, we used a Y408F mutant enzyme to obtain the complex structures reported here. Therefore, the distance between the Tyr⁴⁰⁸ and the glycosidic oxygen could not be determined; however, the distances of 4.55 Å for the HA₆ complex and 4.63 for the HA₄ complex between Phe⁴⁰⁸ and the glycosidic oxygen, O4, are consistent with the proposed role of Tyr⁴⁰⁸. Furthermore, the corresponding distances based on the modeled position of Tyr⁴⁰⁸ (Table II) are 3.18 and 3.10 Å. There are two other residues, Arg⁴⁶² and Arg⁴⁶⁶, that are in close proximity to the glycosidic oxygen and could in principle serve as acids to donate hydrogen to the glycosidic oxygen (Fig. 3). Their possible contribution to catalysis cannot be discarded although the p*K*_a of Arg is significantly higher than that of Tyr so that their participation seems unlikely.

Hydrogen Exchange with Microenvironment—In the catalytic process described above, the enzyme molecule loses one hydrogen from Tyr⁴⁰⁸ and gains another one at His³⁹⁹. As the final step, the hydrogen balance needs to be restored for the enzyme to return to its original state and be ready for the next round of catalysis. There is no evidence in the structure of hydrogen channeling using ordered water molecules or resi-

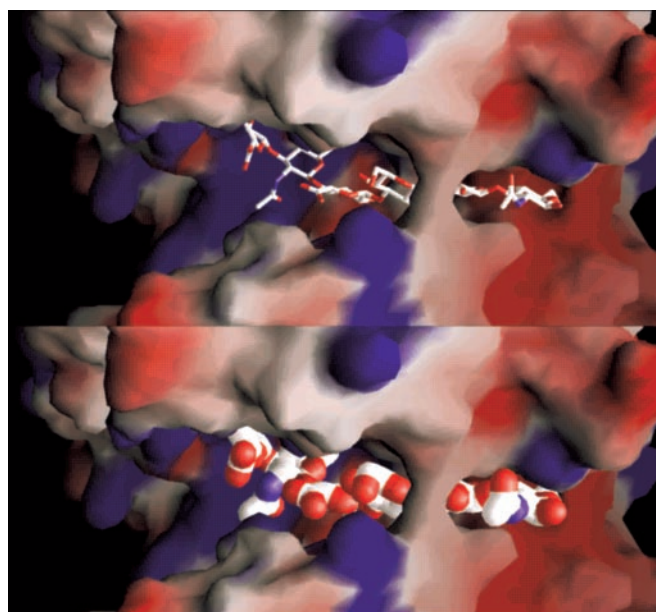


FIG. 6. Electrostatic potential distribution in the catalytic cleft. The positive potential was shown in blue and negative potential in red. The majority of the cleft is highly positively charged (*middle and the left side*), whereas at the product-releasing end of the cleft a negative patch is clearly present (*right side of the cleft*). The hydrophobic patch is hidden beneath the bridge over the substrate. The bridge over the substrate cleft facilitates the threading of the substrate through the cleft. The flexibility analysis (see the text) of the enzyme suggests that this bridge is formed after substrate binding, and likely only during the catalysis. *Top*, bound hexasaccharide hyaluronan shown as sticks. *Bottom*, space filling hexasaccharide hyaluronan bound in the cleft.

dues of the enzyme. The closest structured water molecules, Wat³ and Wat⁴, identified in the electron density in the proximity of His³⁹⁹ are more than 6 Å away (Table II and Fig. 3*a*). No structured waters were identified anywhere close to the Phe⁴⁰⁸ of Y498F enzyme complexes. Therefore, the hydrogens are likely equilibrated using the unstructured water microenvironment present in the cleft of the enzyme.

For the next round of catalysis to take place, the enzyme also needs to release the generated disaccharide product from the active site. This can happen by either translocation of the remaining polymeric HA substrate to the catalytic position by an advance by one disaccharide unit toward its reducing end (considered more likely) or by the release of the substrate from the cleft thereby allowing the binding of a new substrate molecule to the enzyme.

Disaccharide Product Release—At the HA1 position in the cleft, there are three negatively charged residues, Glu³⁸⁸, Asp³⁹⁸, and Thr⁴⁰⁰, grouped together at the bottom of the cleft surface, directly opposite the Phe³⁴³ amino acid residue of the hydrophobic patch (Fig. 4). These residues are responsible for the generation of a patch of negative potential (negative patch) in the area of the cleft where the HA1 disaccharide of the electronegative substrate binds (Fig. 6). The presence of this patch is likely not coincidental but is probably important for the function of the enzyme. Most likely, after catalysis when the disaccharide product is cleaved off from the polymeric HA substrate chain, this product is directly located in this potential. As a consequence, the product is electrostatically repelled from the cleft. Such behavior rationalizes the release of the product from the cleft. The electronegative patch simply facilitates this process and frees up this part of the cleft, making the enzyme ready for the next round of catalysis.

Translocation of the Substrate and the Processive Mode of Action of the Enzyme—After the release of the disaccharide

product, there remains a truncated polymeric HA in the cleft that can become a substrate for further degradation. One possibility is that the substrate leaves the cleft and the enzyme binds again a new or the same hyaluronan molecule into the catalytic cleft (random endolytic or exolytic binding and then cleavage). Alternatively, the molecule already bound in the cleft could be translocated in the cleft by one disaccharide unit toward the reducing end for the next round of catalysis (subsequent processive exolytic binding and cleavage of unsaturated hyaluronan disaccharides by the enzyme). The latter seems to be the case as shown by the biochemical evidence collected for the similar *S. agalactiae* hyaluronate lyase enzyme (47). As the *S. pneumoniae* enzyme is very similar in its sequence and structural and functional properties to the *S. agalactiae* enzyme from the same genus, it is reasonable to assume that this enzyme behaves in the same way. The overall sequence identity between the two enzymes is 51%, and sequence homology is 66%. In addition, the structures of both enzymes show a high degree of similarity, especially in the active site area (19, 22) (Fig. 5c). In this processive mechanism of action of hyaluronate lyase, the enzyme probably binds randomly to HA and cleaves it into two pieces (random endolytic or exolytic cleavage), of which only the one at the reducing end leaves the cleft (as described for the disaccharide product). The remaining chain undergoes translocation in the cleft by one disaccharide unit, and the catalysis goes on to generate another disaccharide unit and so on until the chain is fully degraded (exolytic processive degradation) (Fig. 5a).

To achieve translocation of a polymeric substrate in the binding cleft, an essential component of the processive mechanism, several main factors need to be in place as follows: (i) complementary interfaces between the processive enzyme and the substrate and appropriate shape of the binding cleft allowing for easy substrate translocation or sliding; (ii) correct energetic balance of substrate-enzyme interactions allowing for the substrate remaining to be associated with the enzyme after catalysis but also retaining the ability to move along the cleft, a sliding mechanism; (iii) mechanism allowing the enzyme to locate the site of catalysis (location of the β 1,4-glycosidic bond to be broken) on the substrate during the translocation/sliding process of the hyaluronan substrate (48); and finally (iv) a mechanism for the release of the product of the reaction, a disaccharide of HA for this hyaluronate lyase, to make room for the remaining polymer to be translocated and for further catalysis to go on. For pneumococcal hyaluronate lyase, all these factors are satisfied. The cleft where the substrate binds is long, straight, deep enough, and wide enough to easily accommodate the polymeric chain of HA, and the shapes of HA and the cleft are complementary to one another (Fig. 6). The interactions between the residues of the cleft and the substrate are in general primarily based on interactions of charged electropositive residues lining the sides of the cleft with the electronegative substrate (Fig. 6). There are numerous interactions of that sort between the enzyme residues and the substrate, which likely allows for moderate binding affinity for the substrate generated not by a few strong and specific interactions but by a multitude of different, small binding interactions as also observed for other processive enzymes (48). These interactions are strong enough to bind and to keep the substrate in place in the cleft; however, they are also weak enough to allow the sliding/translocation of the polymer along the straight cleft to advance the substrate and to move it into the new catalytic position. Electrostatic interactions are known not to have significant directionality associated with them, unlike hydrogen bonds, for example, and can more easily allow for shifts maintaining their interactions. Once such a translocation takes

place, a group of hydrophobic residues directly adjacent to the three catalytic residues, termed by us as a hydrophobic patch composed of Trp²⁹¹, Trp²⁹², and Phe³⁴³, precisely positions the substrate. Especially, the positioning of the region in the close proximity to the glycosidic β -1,4 bond between the terminal disaccharide to be freed from the polymer and the remaining part of HA is essential for catalysis. This interaction is based on hydrophobic interactions of the sugar rings of the substrate and similar aromatic and hydrophobic structures of the side chains of the above-mentioned residues. Specifically, HA1 disaccharide interacts with Phe³⁴³ and partially with Trp²⁹¹, whereas Trp²⁹² interacts with HA2; all residues utilize hydrophobic interactions. Finally, the negative patch located at the reducing end of the substrate/cleft provides a mechanism for the release of the product of the reaction, the unsaturated disaccharide unit of hyaluronan (Figs. 4 and 5).

Direction of Hyaluronan Degradation—The processive nature of hyaluronan degradation leads to the question whether this degradative process is performed from the reducing end of the substrate to the nonreducing end or vice versa. Our current structural report including the complexes of tetra- and hexasaccharide HA with the enzyme and our previous work (16, 19) on the complex structures with the disaccharide products suggests that the degradation takes place from the reducing to the nonreducing end of hyaluronan. The current structures clearly show that the cleavage of the β -1,4-glycosidic bond between HA1 and HA2 disaccharide units of the tetra- and hexasaccharide substrates will produce an unsaturated disaccharide unit of HA at the reducing end of the chain and a tetrasaccharide (for the hexasaccharide complex) or a disaccharide (for the tetrasaccharide complex). The tetrasaccharide product of the degradation of the hexasaccharide can be further degraded to disaccharides, whereas the disaccharide product of tetrasaccharide degradation cannot be further degraded (17). The translocation of the substrate in the reducing end direction advances HA polymer to the new degradation position. In this position the HA2 disaccharide took the place of the cleaved HA1 disaccharide, and HA3 took the place of HA2 (Figs. 4 and 5). In addition, the presence of the negative patch at the reducing end of bound HA chain further identifies this reducing end as the releasing end of the substrate. The structures of the hyaluronate lyase enzyme with the bound product of degradation also support this analysis because no bound product was found at the HA3 non-reducing position in the cleft (16, 19). The possibility of the degradation of HA in the opposite direction from the non-reducing to the reducing end is clearly not supported by the current structures of the complexes or by our earlier studies.

Comparison of Hyaluronan Degradation to the Degradation of Dermatan Sulfate, Chondroitin Sulfate, and Alginate—The degradation of polysaccharides by polysaccharide lyases such as hyaluronate lyase has been investigated for some time by biochemical and structural methods (e.g. Refs. 49 and 50). Recent structural investigations of *F. heparinum* chondroitin AC lyase (20) and *Sphingomonas* species alginate lyase A1-III (21) provided some additional insight into this process. The overall fold of the *F. heparinum* chondroitin AC lyase (20) is similar to that of *S. pneumoniae* hyaluronate lyase consisting of two domains, a α -helical and a β -sheet domain. The α -helical domain contains a similar elongated cleft where the polymeric sugar molecules bind and are cleaved. Several scenarios were proposed for the chondroitin AC lyase mechanism of dermatan sulfate, chondroitin sulfate, and hyaluronan degradation, and these mechanisms involve His²²⁵ and Tyr²³⁴, residues corresponding to His³⁹⁹ and Tyr⁴⁰⁸, respectively, of the pneumococcal hyaluronate lyase. The homologous residue to Asn³⁴⁹ of the

FIG. 7. Stereo view of the superposition of the minimum and the maximum projection structures of hyaluronate lyase. Motions described by eigenvectors 1 (*a*) and 3 (*b*) are shown. *Green* and *red* coils represent the minimum and maximum projections, respectively. *a*, α -domain movement regulating the access to the cleft. $C\alpha$ atoms of the positive patch residues are drawn as *magenta spheres*. Residues from the active center (Asn³⁴⁹, Tyr⁴⁰⁸, and His³⁹⁹) and from the negative patch (Glu³⁸⁸, Asp³⁹⁸, and Thr⁴⁰⁰) are drawn as *blue* and *yellow spheres*, respectively, and labeled. *b*, opening up and closing of the cleft. Movement between the two domains, opening and closing a pocket is shown (His³⁹⁹, drawn as a *sphere*). Selected residues are shown as *cyan spheres* and labeled (see Table III for distance details between these residues).

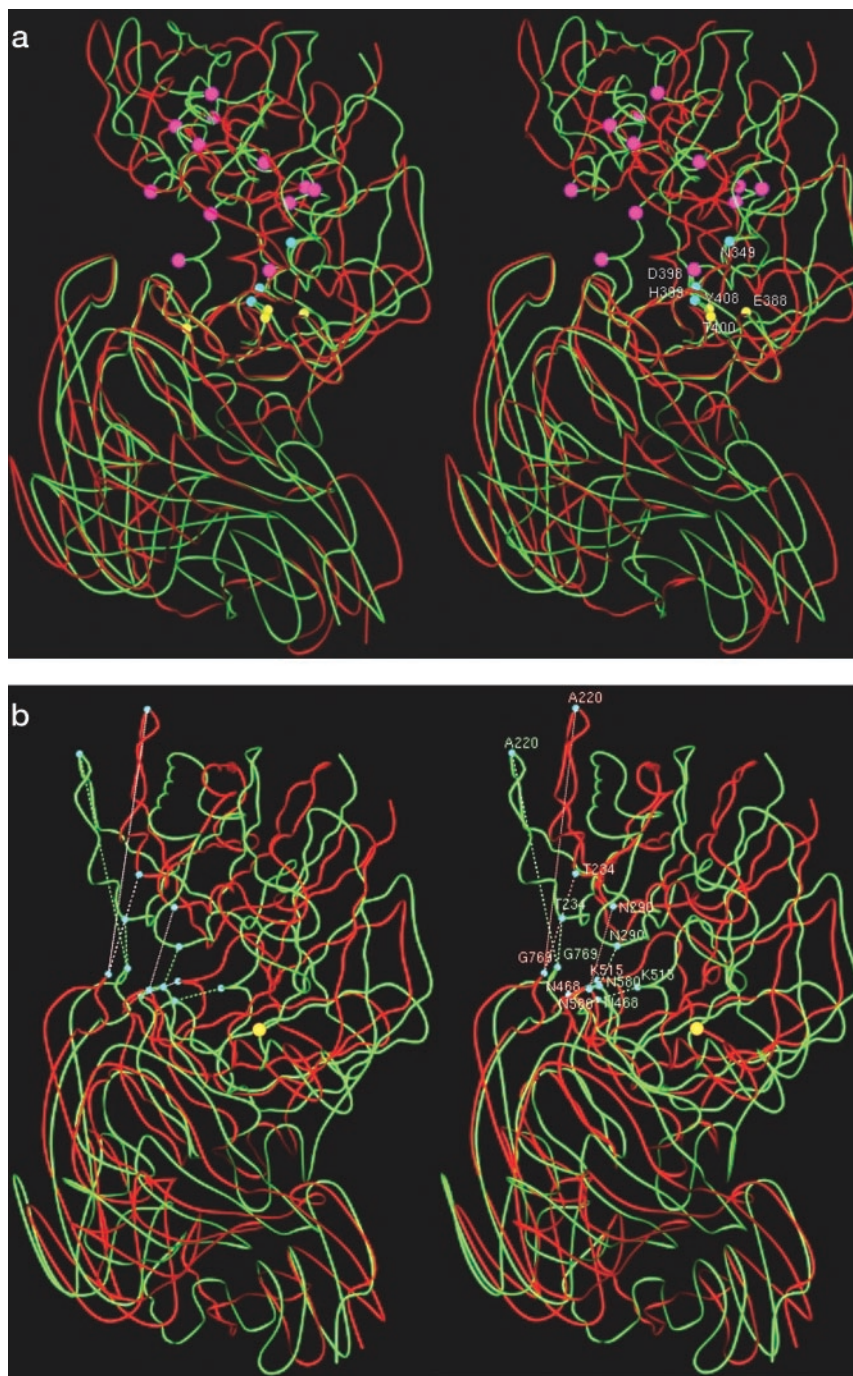


TABLE III
Distances between selected residues of the minimum and maximum projection structures of eigenvector 3 resulting from the CONCOORD simulations

Residues involved	Minimum projection distance	Maximum projection distance
	(Å)	
Thr ²³⁴ -Gly ⁷⁶⁹	10.9	14.0
Asn ⁵⁸⁰ -Asn ²⁹⁰	6.6	11.6
Ala ²²⁰ -Gly ⁷⁶⁹	29.3	36.8
Asn ⁴⁶⁸ -Lys ⁵¹⁵	10.0	11.6

pneumococcal hyaluronate lyase, Asn¹⁷⁵, has not been directly implicated in the degradation mechanism for chondroitin AC lyase by Huang *et al.* (20), although modeling studies and the complex structures of the AC lyase showed that this residue could interact with the carboxylate group of the C-5 of all

substrates (20). Also, the residue homologous to Arg⁴⁶² of *S. pneumoniae* lyase, Arg²⁸⁸, was implicated in the chondroitin AC lyase mechanism as possibly a general acid acting as a donor of hydrogen to the glycosidic oxygen during the cleavage of this bond or as a charge-neutralizing residue for the enolate anion intermediate formed during catalysis. Our analysis of the active site of *S. pneumoniae* hyaluronate lyase does not support such role of Arg⁴⁶² for the pneumococcal lyase. Even though Arg⁴⁶² is in close proximity to the glycosidic oxygen of hyaluronan (Table II), its pK_a for hydrogen donation is significantly higher than that of Tyr⁴⁰⁸, and therefore the latter residue is more likely to participate in this way. Mutation of the homologous residue to Arg⁴⁶² for the hyaluronate lyase from *S. agalactiae*, Arg⁵⁴², decreased but did not abolish the activity of this enzyme (51) supporting our conclusions. This Arg may have a structural role or be involved in substrate

binding; either of these functions would reasonably explain the reduced enzyme activity on its mutation.

Another recently studied polysaccharide degrading enzyme is alginate lyase. The overall fold of the *Sphingomonas* species alginate lyase A1-III elucidated structurally only recently (21) is similar to that of the α -domain of *S. pneumoniae* hyaluronate lyase, but the β -sheet domain is not present in this enzyme. The α -helical domain also supports the formation of a similar elongated substrate-binding cleft to that of the pneumococcal lyase. For the alginate lyase A1-III a Tyr²⁴⁶, homologous to Tyr⁴⁰⁸ of the pneumococcal lyase, was suggested to act as both a base withdrawing hydrogen from the C-5 of alginate and as an acid donating hydrogen to the glycosidic oxygen (21). Although this may be possible for the alginate lyase, we do not see evidence for such behavior with hyaluronate lyase in our complex structures nor from earlier studies (9, 13, 17, 19).

Protein Flexibility of Hyaluronate Lyase and Its Functional Implications—Computational studies often can enable correlations between mobility of proteins or their segments and specific functions (52). Concerted motions involving protein segments may be deduced from ED analysis of molecular dynamics (MD) simulations (52–54). In the case of pneumococcal hyaluronate lyase, its size precludes the realistic calculation of MD trajectories at biologically relevant time scales. However, good qualitative agreement between the results of ED analyses of MD trajectories and the results of analysis of CONCOORD software generated structures has been obtained (see “Experimental Procedures”). We therefore applied the CONCOORD/ED methodology to seek independent support for the proposed roles of the dynamical features of the enzyme, in particular in the region of the binding cleft and its catalytic region.

The largest amplitude concerted fluctuation, mathematically described by the first eigenvector, is a rotation/twisting motion of the whole α -domain relative to the top half of the β -domain (Fig. 1). Concomitantly, the bottom half of the β -domain rotates in the opposite direction, relative to the top half of that domain. Fig. 7a shows the superimposition of the minimum and maximum projections for this first eigenvector. These projection structures correspond to the two extreme structures associated with this mode of fluctuation. The intra- β -domain motion seems to be of little functional consequence because the interface between the two dynamically independent portions of the β -domain lies distant to the active site. However, the residues from the positively charged majority of the binding cleft of the α -domain of the enzyme (a positive patch) are particularly mobile relative to residues from the active center and the negative patch. This is consistent with the previous hypothesis (19) that the mobility of the positive patch is related to drawing the ligand into the binding cleft.

Another major motion of the hyaluronate lyase is also related to an opening/closing of the substrate-binding cleft and is described by eigenvector 3. Fig. 7b shows the superimposition of the minimum and maximum projections for this mode of concerted fluctuation. The change of the distance between selected residues involved in the movement is shown in Table III. The residues from the active site and from the negative patch, whose relative orientation did not change significantly with the motion described by the first eigenvector, exhibit significant relative positional shifts along the motion described by eigenvector 3. This finding is interesting given the obvious need of the enzyme to release the electronegative disaccharide product of degradation from the active site in order to enable relocation and further processing of the remaining polysaccharide. In addition, there is evidence for the mobility, relative to the α -domain, of two loops from the β -domain, which are involved

in the cleft formation (described earlier). For example, Asn⁵⁸⁰, which is located at the tip of one of the loops from the β -domain, shows a relatively large fluctuation (Table III). As described above and supported by the earlier kinetic analysis (17), the N508G mutant showed significantly higher activity when compared with the wild type enzyme, confirming the importance of this loop to catalysis. Therefore, the flexibility analysis suggests that this opening/closing motion of the enzyme is directly relevant not only to hyaluronan binding but also to the catalysis itself.

Conclusions and Biological Implications—The current structures of hyaluronate lyase complexes with substrates enable us to draw conclusions related to the functional properties of the enzyme. The mechanism of catalysis was well established as proton acceptance and donation. The comprehensive analysis of the entire process of hyaluronan degradation was proposed including the irreversible release of the disaccharide product and the nature of the processive mechanism of this important biological process. The residues involved in substrate binding, precise positioning for catalysis, catalysis itself, the release of the product, and the translocation of the remaining substrate were clearly identified, and their contribution to the entire degradation process was described. The nature of the processive behavior of hyaluronate lyase described here is likely relevant to other processive enzymes. Finally, we presented simulated molecular and essential dynamics analyses that shed light on the aspects of the function of the enzyme that would be inaccessible to evaluation of static crystal structures.

Acknowledgments—Diffraction data for this study were collected at Advanced Photon Source, Structural Biology Center at the beamline 19-BM, Argonne National Laboratory (supported by the United States Department of Energy under Contract W-31-109-ENG-38).

REFERENCES

- Mufson, M. A. (1990) in *Principles and Practice of Infectious Diseases* (Mandell, G. L., Douglas, R. G., Jr., and Bennett, J. E., eds) Churchill Livingstone, New York
- Stool, S. E., and Field, M. J. (1989) *Pediatr. Infect. Dis. J.* **8**, S11–S14
- Berry, A. M., Lock, R. A., Thomas, S. M., Rajan, D. P., Hansman, D., and Paton, J. C. (1994) *Infect. Immun.* **62**, 1101–1108
- Lock, R. A., Paton, J. C., and Hansman, D. (1988) *Microb. Pathog.* **5**, 461–467
- Paton, J. C., Berry, A. M., Lock, R. A., Hansman, D., and Manning, P. A. (1986) *Infect. Immun.* **54**, 50–55
- McDaniel, L. S., Sheffield, J. S., DeLucchi, P., and Briles, D. E. (1991) *Infect. Immun.* **59**, 222–228
- Jedrzejewski, M. J. (2001) *Microbiol. Mol. Biol. Rev.* **65**, 187–207
- Berry, A. M., and Paton, J. C. (1996) *Infect. Immun.* **64**, 5255–5262
- Li, S., Kelly, S. J., Lamani, E., Ferraroni, M., and Jedrzejewski, M. J. (2000) *EMBO J.* **19**, 1228–1240
- McCourt, P. A. G. (1999) *Matrix Biol.* **18**, 427–432
- Toole, B. P., Goldberg, R. L., Chi-Rosso, G., Underhill, C. B., and Orkin, R. W. (1984) in *The Role of Extracellular Matrix in Development* (Trelstad, R. C., ed) Alan R. Liss, Inc., New York
- Laurent, T. C., and Fraser, R. E. (1992) *FASEB J.* **6**, 2397–2404
- Jedrzejewski, M. J. (2000) *Crit. Rev. Biochem. Mol. Biol.* **35**, 221–251
- Courtiss, E. H., Ransil, B. J., and Russo, J. (1995) *Plast. Reconstr. Surg.* **95**, 876–883
- Menzel, E. J., and Farr, C. (1998) *Cancer Lett.* **131**, 3–11
- Ponnuraj, K., and Jedrzejewski, M. J. (2000) *J. Mol. Biol.* **299**, 885–895
- Kelly, S. J., Taylor, K. B., Li, S., and Jedrzejewski, M. J. (2001) *Glycobiology* **11**, 297–304
- Li, S., Taylor, K. B., Kelly, S. J., and Jedrzejewski, M. J. (2001) *J. Biol. Chem.* **276**, 15125–15130
- Li, S., and Jedrzejewski, M. J. (2001) *J. Biol. Chem.* **276**, 41407–41416
- Huang, W., Boju, L., Tkalec, L., Su, H., Yang, H. O., Gunay, N. S., Linhardt, R. J., Kim, Y. S., Matte, A., and Cygler, M. (2001) *Biochemistry* **40**, 2359–2372
- Yoon, H. J., Hashimoto, W., Miyake, O., Murata, K., and Mikami, B. (2001) *J. Mol. Biol.* **307**, 9–16
- Jedrzejewski, M. J., Mewbourne, R. B., Chantalat, L., and McPherson, D. T. (1998) *Protein Expression Purif.* **13**, 83–89
- Jedrzejewski, M. J., Chantalat, L., and Mewbourne, R. B. (1998b) *J. Struct. Biol.* **121**, 73–75
- Ducruix, A., and Giege, R. (eds) (1992) *Crystallization of Nucleic Acids and Proteins: A Practical Approach*, Oxford University Press, New York
- McPherson, A. (1999) *Crystallization of Biological Molecules*, Cold Spring Harbor Laboratory Press, Cold Spring Harbor, New York
- Otwinowski, Z., and Minor, W. (1997) *Methods Enzymol.* **276**, 307–326
- Brunger, A. T. (1992) *Nature* **355**, 472–474
- Brunger, A. T., and Warren, G. L. (1998) *Acta Crystallogr. Sect. D Biol.*

- Crystallogr.* **54**, 905–921
29. Jones, T. A., Zhou, J. Y., Cowan, S. W., and Kjeldgaard, M. (1991) *Acta Crystallogr. Sect. A* **47**, 110–119
30. Rice, L. M., and Brunger, A. T. (1994) *Proteins Struct. Funct. Genet.* **19**, 277–290
31. Kleywegt, G. J., and Jones, T. A. (1996) *Acta Crystallogr. Sect. D Biol. Crystallogr.* **52**, 829–832
32. Laskowski, R. A., MacArthur, M. W., Moss, D. S., and Thornton, J. M. (1993) *J. Appl. Crystallogr.* **26**, 283–291
33. de Groot, B. L., van Aalten, D. M., Scheek, R. M., Amadei, A., Vriend, G., and Berendsen, H. J. (1997) *Proteins Struct. Funct. Genet.* **29**, 240–251
34. de Groot, B. L., Vriend, G., and Berendsen, H. J. (1999) *J. Mol. Biol.* **286**, 1241–1249
35. Kleinjung, J., Bayley, P., and Fraternali, F. (2000) *FEBS Lett.* **470**, 257–262
36. Berendsen, H. J. C., van der Spoel, D., and van Drunen, R. (1995) *Comp. Phys. Comm.* **91**, 43–56
37. Lindahl, E., Hess, B., and van der Spoel, D. (2001) *J. Mol. Model.* **7**, 306–317
38. Amadei, A., Linssen, A. B., and Berendsen, H. J. (1993) *Proteins Struct. Funct. Genet.* **17**, 412–425
39. Carson, M. (1997) *Methods Enzymol.* **277**, 493–505
40. Nicholls, A., Sharp, K. A., and Honig, B. (1991) *Proteins Struct. Funct. Genet.* **11**, 281–296
41. Kraulis, P. J. (1991) *J. Appl. Crystallogr.* **24**, 946–950
42. Park, Y., Cho, S., and Linhardt, R. J. (1997) *Biochim. Biophys. Acta* **1337**, 217–226
43. Shimada, E., and Matsumura, G. (1980) *J. Biochem. (Tokyo)* **88**, 1015–1023
44. Scott, J. E., and Heatley, F. (1999) *Proc. Natl. Acad. Sci. U. S. A.* **96**, 4850–4855
45. Pritchard, D. G., Lin, B., Willingham, T. R., and Baker, J. R. (1994) *Arch. Biochem. Biophys.* **315**, 431–437
46. Gerlt, J. A., and Gassman, P. G. (1992) *J. Am. Chem. Soc.* **114**, 5928–5934
47. Baker, J. R., and Pritchard, D. G. (2000) *Biochem. J.* **1**, 465–471
48. Breyer, W. A., and Matthews, B. W. (2001) *Protein Sci.* **10**, 1699–1711
49. Gacesa, P. (1987) *FEBS Lett.* **212**, 199–202
50. Greiling, H., Stuhlsatz, H. W., Eberhard, T., and Eberhard, A. (1975) *Connect. Tissue Res.* **3**, 135–139
51. Pritchard, D. G., Trent, J. O., Li, X., Zhang, P., Egan, M. L., and Baker, J. R. (2000) *Proteins Struct. Funct. Genet.* **40**, 126–134
52. Mello, L. V., van Aalten, D. M. F., and Findlay, J. B. C. (1997) *Protein Eng.* **10**, 381–387
53. Mello, L. V., van Aalten, D. M. F., and Findlay, J. B. C. (1998) *Biochemistry* **37**, 3137–3142
54. Dahl, S. G., Edvardsen, O., and Sylte, I. (1991) *Proc. Natl. Acad. Sci. U. S. A.* **88**, 8111–8115
55. Brunger, A. T., and Krukowski, A. (1990) *Acta Crystallogr. Sect. A* **46**, 585–593